ELSEVIER

Physica B 221 (1996) 437–444

PHYSICA B

The use of X-ray standing waves and evanescent-wave emission to study buried strained-layer heterostructures

T.-L. Lee[a,*], Y. Qian[a,b], P.F. Lyman[a], J.C. Woicik[c], J.G. Pellegrino[c], M.J. Bedzyk[a,b]

[a]*Department of Materials Science and Engineering and Materials Research Center, Northwestern University, Evanston, IL 60208, USA*
[b]*Materials Science Division, Argonne National Laboratory, Argonne, IL 60439, USA*
[c]*National Institute of Standards and Technology, Gaithersburg, MD 20899, USA*

Abstract

A heteroepitaxial structure consisting of 1 ML InAs grown on GaAs(0 0 1) and then capped with 25 Å GaAs was examined by the X-ray standing wave (XSW) method. By monitoring the In L fluorescence while scanning through the GaAs(0 0 4) Bragg reflection, the perpendicular strain within the InAs layer was directly measured to be 7.7%, which is in good agreement with macroscopic elasticity theory (7.3%). We also demonstrate that, combined with the evanescent-wave-emission effect, the XSW method can be used to measure the strain-induced displacement of the cap layer in the growth direction.

The progress in crystal growth techniques in the past two decades has made it possible to manufacture novel devices by synthesizing artificially layered materials built up of structurally and chemically dissimilar constituents. InAs/GaAs, for instance, can be made to have a band gap within the range of interest for optical fiber communication. In a pseudomorphically grown heterostructure, the buried film is constrained to have the same lattice parameters as the substrate in the plane parallel to the film, while it is free to relax in the growth direction, resulting in tetragonal distortion of the unit cell. It has been shown [1] that this strain, induced by lattice misfit, has a number of effects on the stability, growth mode and surface morphology of the heterolayer. It also plays a crucial role in determining the optical and electronic properties of the film.

Based on the macroscopic continuum elasticity theory, for cubic materials with the buried film parallel to the (0 0 1) plane, the strain normal to the (0 0 1) plane $\varepsilon_\perp$ is related to the in-plane strain $\varepsilon_\parallel$ by

$$\varepsilon_\perp = -2\frac{C_{12}}{C_{11}}\varepsilon_\parallel, \tag{1}$$

where the C_{ij} are the bulk elastic constants for the embedded material. For InAs, these constants are $C_{11} = 8.329 \times 10^{11}$ and $C_{12} = 4.526 \times 10^{11}$ dyn/cm^2 [2] and a lattice misfit of $\varepsilon_\parallel = -6.7\%$ exists between InAs and GaAs. Thus, Eq. (1) predicts a strain of $\varepsilon_\perp = 7.3\%$ for a thin pseudomorphic InAs layer buried in GaAs. Recent experimental evidence from Brandt et al. [3], based on a high-resolution electron microscopy (HREM) analysis, showed good agreement with Eq. (1) for a 3 ML InAs sample, but gave a much larger $\varepsilon_\perp$ (12.46%) for a sample with one monolayer of InAs. This discrepancy has drawn attention to the issue of whether macroscopic elasticity theory can correctly describe the strain in an ultra-thin film. Using high-resolution X-ray diffraction (HRXRD) and XSW methods, Giannini et al. [4] investigated the interfacial profile of 1.2 ML InAs. Their results can be shown to be consistent with the assumption of

*Corresponding author.

SSDI 0921-4526(95)00964-7

$\varepsilon_\perp = 7.3\%$. Bernard and Zunger [5] performed a local-density total-energy calculation for the same system. Their result did not indicate an anomalous elastic strain in the one monolayer limit. Using back-reflection X-ray standing waves (BRXSW), Woicik et al. [6] have measured the indium position to be 1.64 Å above the last substrate arsenic plane for the 1 ML case, which corresponds to an 8.2% perpendicular strain and is therefore in reasonable agreement with the elasticity theory.

In the present X-ray standing wave study, we directly measured the strain in 1 ML of InAs buried in GaAs (0 0 1) by precisely measuring the indium position relative to the underlying GaAs substrate unit cell. Furthermore, we demonstrate that by adding depth selectivity to the XSW measurement, one can measure the strain-induced displacement of the thin GaAs cap layer in the growth direction. This depth selectivity, which is achieved by the evanescent-wave-emission effect, is also used to characterize the homoepitaxy of the GaAs buffer layer and the cap layer.

Our GaAs/1 ML InAs/GaAs(0 0 1) sample (Figs. 1 and 2) was prepared by molecular beam epitaxy (MBE) at the National Institute of Standards and Technology. An electronic grade semi-insulating GaAs(0 0 1) substrate was chemically cleaned and then etched using a conventional sulfuric acid/hydrogen peroxide/deionized water solution. The surface oxide layer was desorbed in the MBE chamber at a temperature of 580 °C in the presence of an arsenic flux. Throughout the MBE growth the arsenic shutter was left open. The gallium and indium effusion cells were shuttered with a 3 s pause step between the growth of the successive layers, in order to improve the interface. A 0.5 μm GaAs buffer layer was deposited at a substrate temperature linearly ramped from 580 °C to 480 °C. The growth of the InAs layer and the 25 Å GaAs cap layer took place at 480 °C. After deposition of the GaAs cap layer, the sample was allowed to cool to room temperature. The arsenic shutter was left open until the sample temperature fell below 400 °C.

The XSW experiments were carried out on a 2-circle diffractometer at beamline X15A of the National Synchrotron Light Source (NSLS) (Fig. 3). During the scan of a pair of Si(0 0 4) monochromator crystals through the GaAs(004) Bragg reflection at photon energy $E_\gamma = 6.00$ keV the fluorescence spectra and reflectivity were recorded simultaneously [7]. The fluorescent X-rays were collected over a limited angular range. The lower limit α_ℓ of the emission takeoff angle is defined by the sample surface ($\alpha_\ell = 0$) and the upper limit α_u is defined by a slit aligned parallel to the sample surface and positioned between the sample and the solid-state Si(Li) fluorescence detector. α_u is adjustable with an accuracy of $\pm 0.1°$. The sample was kept in a helium atmosphere throughout the X-ray measurements in order to eliminate Ar Kα from the fluorescence spectrum and to reduce the attenuation of the low energy fluorescent X-rays.

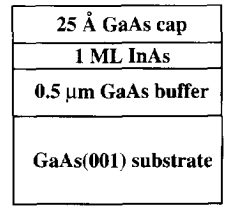

Fig. 1. Schematic of GaAs/InAs/GaAs(001) heterostructure with thicknesses.

The first (0 0 4) measurement was performed at $\alpha_u = 10$ in order to obtain bulk structural information, which will be later compared to the data collected at various low-takeoff angles. Fig. 4 shows the GaAs(0 0 4) rocking curve and the In L fluorescence yield as a function of incident angle θ. Based on von Laue and Ewald's dynamcial diffraction theory [8], the fluorescence yield $Y(\theta)$ stimulated by the X-ray standing wave created at the $\boldsymbol{H}$ Bragg reflection can be described as

$$Y(\theta) = Y_{OB}[1 + R(\theta) + 2\sqrt{R(\theta)} f_H \cos(v(\theta) - 2\pi P_H)]\, L(\theta) \quad (2)$$

where Y_{OB} is the off-Bragg fluorescence yield, $R(\theta)$ is the reflectivity and $v(\theta)$ is the phase difference between the incident and the reflected plane waves. $L(\theta)$ is the effective thickness accounting for the attenuation of both the primary X-ray field and the secondary fluorescent X-rays. $L(\theta)$ is fixed at unity if the atoms under investigation are at or near the surface (e.g., the indium atoms in our case). The amplitude f_H and phase P_H of the fluorescence modulation, which are referred to as the coherent fraction and the coherent position, measure the width and the average position of the atomic spatial distribution along the $\boldsymbol{H}$ direction, respectively. For the 1 ML InAs strained layer, the (004) indium coherent position is directly related to the perpendicular strain $\varepsilon_\perp$ in the heterolayer by

$$\varepsilon_\perp = (P_{004}\, a_{GaAs} - a_{InAs})/a_{InAs}. \quad (3)$$

This expression assumes that indium occupies only one ordered position along the (004) direction. ($a_{GaAs} = 5.653$ Å and $a_{InAs} = 6.058$ Å are the lattice constants for GaAs and InAs, respectively.) The indium coherent position, determined by the best fit of Eq. (2) to our data, is $P_{004} = 1.154 \pm 0.01$. This corresponds to an indium position located 1.63 ± 0.01 Å above the last substrate arsenic plane (or 0.22 Å above the nearest GaAs(004) diffraction plane) (see Fig. 2). Based on Eq. (3), the strain

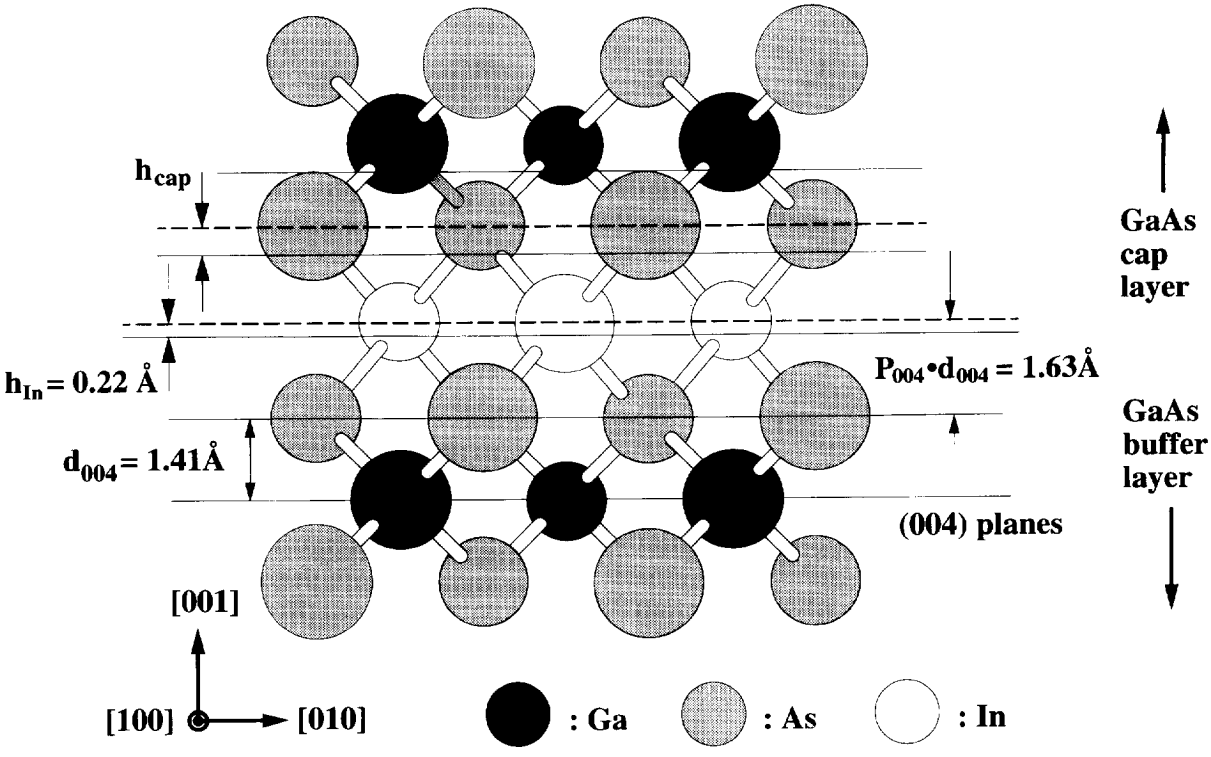

Fig. 2. The [100] projected side view of 1 ML InAs buried between the GaAs cap layer and buffer layer. The solid lines represent the substrate GaAs (004) diffraction planes and the dashed lines indicate the indium position and the position for the arsenic in the cap. h_{In} and h_{cap} are the displacements of the In atoms and the cap As atoms, respectively, with respect to the (004) diffraction planes.

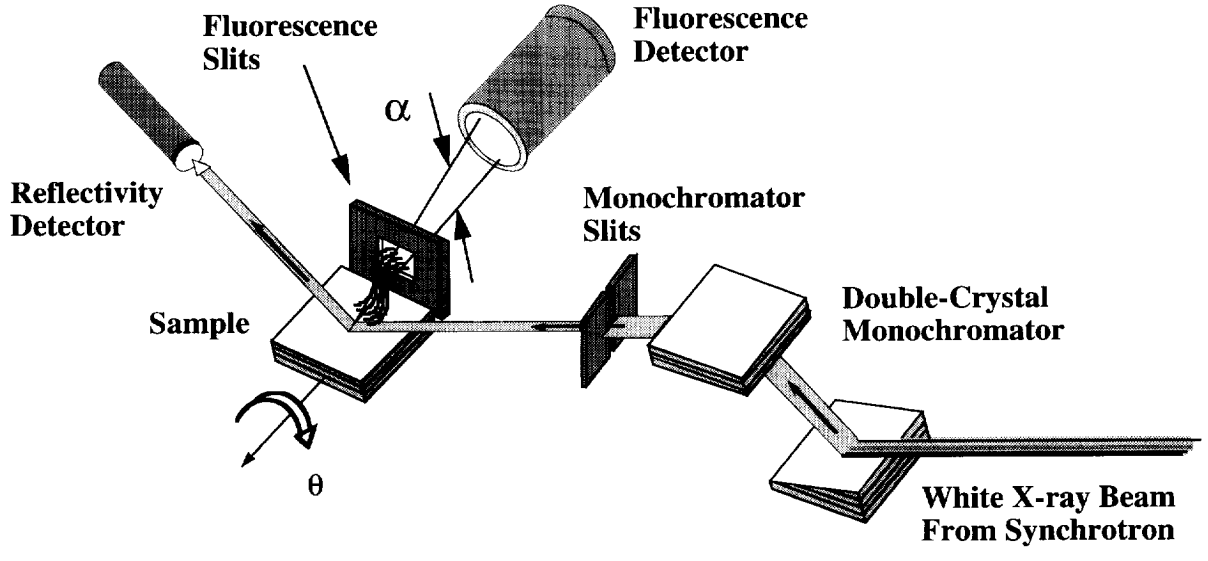

Fig. 3. A depiction of the experimental setup used for collecting XSW data at beamline X15A of NSLS. The fluorescence spectra and reflectivity are simultaneously recorded during the energy scan of a pair of Si(004) monochromator crystals through the GaAs(004) reflection. The fluorescence is collected by an energy-dispersive solid-state detector after passing through a slit which can be used to limit the collected signal to the selected takeoff angle.

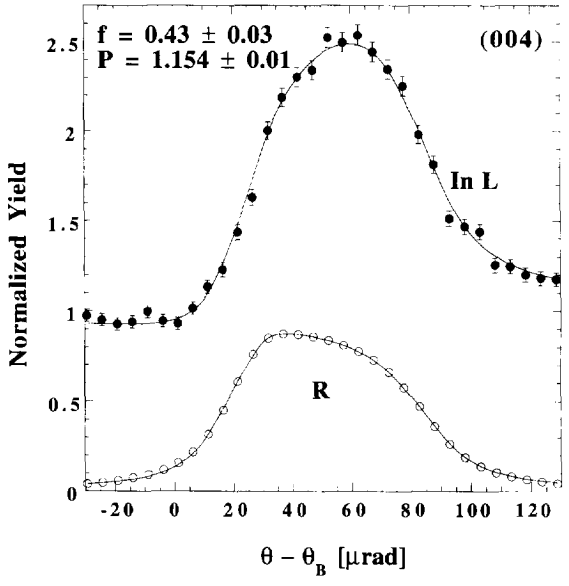

Fig. 4. The experimental XSW data and the best fits (solid lines) to the data points for the normalized In L fluorescence yield and the GaAs(004) reflectivity (R) versus angle θ.

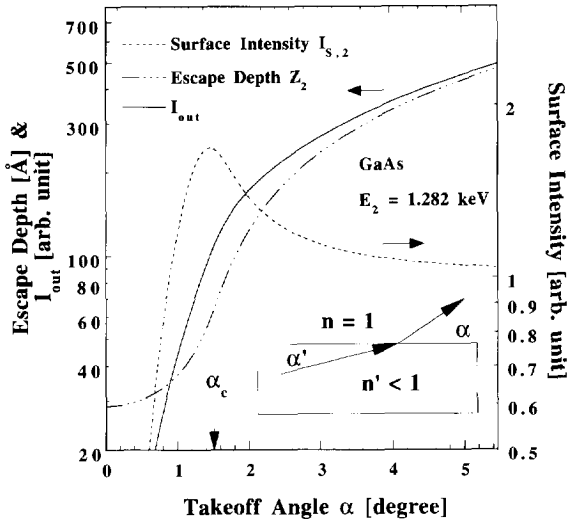

Fig. 5. The calculated angular dependence for the escape depth and the surface intensity for GaAs at As Lα emission energy (1.282 keV). The intensity $I_{out}(\alpha)$ ($= \int_0^{\infty} I_{out}(\alpha, z)dz$) is obtained as the product of the escape depth and the surface intensity curves (see text). The inset shows the emission geometry for the secondary X-rays.

in the InAs layer in the [001] direction is then 7.7%. This is in good agreement with the values predicted by both the macroscopic elasticity theory (7.3%) and the local density total energy calculation (7.7%), and also confirms the BRXSW measurement (8.2%). If the In atom distribution was ideal as depicted in Fig. 2, the In coherent fraction should have been close to the GaAs(004) Debye–Waller factor ($D_{004} = e^{-M} = 0.89$). The relatively low coherent fraction measured for In of $f_{004} = 0.43$ is most likely a result of structural disorder. It should be noted that somewhat less disorder was found in the BRXSW measurement [6].

Another way to measure the strain in a buried film is to consider the displacement of the cap layer in the growth direction with respect to the ideal lattice of the substrate. For instance, using the fact that the X-ray field scattered by the displaced top layer has a phase shift relative to that scattered by the substrate, Tapfer and Ploog [9] have used the Pendellösung effect to study the lattice strain and chemical composition of $GaAs/Al_xGa_{1-x}As/GaAs$ heterostructure. Since this interference effect relies on the shifted film to be a strong diffractor, the thickness of the cap needs to be comparable to the X-ray extinction depth in order to produce a strong modulation and to consequently achieve a reasonable accuracy. For samples with a cap layer thinner than 100 Å this technique becomes insensitive to the strain of the buried film. We will demonstrate, in the second part of this report, that by combining the conventional XSW method and the evanescent-wave-emission effect, one can precisely measure the strain-induced cap displacement and also examine its homoepitaxy for a sample with the cap layer thickness t_c of only 25 Å.

Studying the structural variation in the near-surface region with the XSW method requires an effective way for isolating surface signals from bulk signals. This would typically be accomplished by using photoelectron emission [10, 11]. The conventional fluorescence-based XSW technique, due to its lack of surface sensitivity, presumably would not be considered as an appropriate tool for this kind of measurement. However, one can dramatically reduce the depth probed by fluorescence by employing the evanescent-wave-emission effect demonstrated by Becker, et al. [12]. As shown in the inset of Fig. 5, emitted X-ray are refracted on their way out of the sample, just as if they were travelling into the sample along the reverse path. If the external angle α is at or below the critical angle α_c for the total external reflection, the real part of the internal angle α' goes to zero. Thus, for $\alpha < \alpha_c$ the emission is described by an evanescent wave with an exponentially damped depth measured in nanometers. According to the principle of microscopic reversibility, the optical theory used for describing the more easily visualized evanescent-wave-absorption effect can be directly used to calculate the evanescent-wave-emission effect. Therefore, the intensity I_{out} of a secondary X-ray from a depth z below the surface can be expressed as

a function of takeoff angle α as

$$I_{out}(\alpha, z) \propto I_{s,2}(\alpha)\, e^{-\mu_{z,2}(\alpha) z}, \tag{4}$$

where

$$I_{s,2}(\alpha) = 4\left\{1 + \frac{|\xi(\alpha)|^2}{\sin^2\alpha} + \frac{2\mathrm{Re}(\xi(\alpha))}{\sin\alpha}\right\}^{-1}$$

$$\text{with} \quad \xi(\alpha) = \sqrt{\sin^2(\alpha) - 2(\delta + i\beta)}. \tag{5}$$

$I_{s,2}(\alpha)$ is the E-field intensity at the surface $|E(\alpha, z=0)/E_0|^2$ based on the Fresnel theory. The subscript "2" is used to indicate that the calculations are performed at the secondary fluorescent X-ray energy. The optical constants δ and β are related to the index of refraction n of the specimen by the definition $n = 1 - \delta - i\beta$. The exponential damping factor in Eq. (4) with

$$\mu_{z,2}(\alpha) = \frac{4\pi}{\sqrt{2}\lambda_2}\{[(2\delta - \alpha^2)^2 + 4\beta^2]^{1/2} + 2\delta - \alpha^2\}^{1/2} \tag{6}$$

[13] accounts for the absorption and extinction of the emitted X-rays. Here λ_2 is the wavelength of the fluorescent photon. Notice that $I_{out}(\alpha, z)$ is simply the depth profile of the E-field intensity for an externally excited evanescent wave at this secondary energy. The same profile cannot be easily obtained for an internally excited evanescent wave without applying the microscopic reversibility principle.

Fig. 5 shows the surface intensity $I_{S,2}(\alpha)$ and the escape depth $Z_2(\alpha) = \mu_{z,2}(\alpha)^{-1}$ calculated from Eqs. (4) and (5) for GaAs at As Lα emission energy (1.282 keV). The surface intensity $I_{s,2}(\alpha)$ is zero at $\alpha = 0$, reaches its maximum at the critical angle $\alpha_c = \sqrt{2\delta} = 1.5°$ and then approaches unity at high takeoff angles. For an externally excited evanescent wave, this variation corresponds to the inward motion of the first antinode of the standing wave created above the surface by total external reflection. Since the As L emission line is right above the Ga L_{III} edge (1.116 keV), the surface intensity maximum is suppressed by absorption (without absorption $I_{s,2}(\alpha_c) = 4$). The escape depth $Z_2(\alpha)$, has a minimum value of 29 Å at $\alpha = 0°$ followed by an abrupt rise at $\alpha = \alpha_c$. It eventually approaches $(\sin\alpha)/\mu_{0,2}$ for high takeoff angles, where $\mu_{0,2}$ is the normal absorption coefficient for GaAs. It is this drastic reduction in the escape depth occurring near the critical angle that makes the X-rays emitted deep below the surface unobservable by the fluorescence detector.

By including the attenuation factor $I_{in}(\theta, z)$ for the primary X-rays, we can express the θ and α dependence of the exponentially damped envelope of the standing wave amplitude as

$$y(\theta, \alpha, z) = I_{in}(\theta, z)\, I_{out}(\alpha, z) \propto I_{s,2}(\alpha)\, e^{-[\mu_{z,1}(\theta) + \mu_{z,2}(\alpha)]z}. \tag{7}$$

Based on dynamical diffraction theory [14] the effective linear absorption coefficient $\mu_{z,1}(\theta)$ in Eq. (7) is

$$\mu_{z,1}(\theta) = \frac{\mu_{0,1}}{\sin\theta_B}\left[1 + \frac{F_H''}{F_0''}\left(\frac{E_H(\theta)}{E_0}\right)' + \frac{F_H'}{F_0''}\left(\frac{E_H(\theta)}{E_0}\right)''\right], \tag{8}$$

where $\mu_{0,1}$ is the normal absorption coefficient for the primary X-ray and θ_B is the Bragg angle for the $\boldsymbol{H}$ reflection. $E_H(\theta)/E_0$ is the E-field amplitude ratio. F_H and F_0 are the structure factors for the $\boldsymbol{H}$ and the zeroth-order reflections. The notations prime and double prime used in Eq. (8) represent the real and the imaginary parts of the complex quantities, respectively, and the subscript "1" is used to denote the primary beam. Physically, the first term in Eq. (8) corresponds to normal absorption, the second term corresponds to anomalous absorption, which accounts for the strengthening and diminishing of the photoelectric absorption due to the motion of the standing wave field with respect to the atomic planes. The last term corresponds to the primary extinction effect. The penetration depth $Z_1(\theta) = \mu_{z,1}(\theta)^{-1}$ for the GaAs(004) reflection at $E_\gamma = 6.0$ keV is depicted in Fig. 6. A minimum Z_1 (or extinction depth) of 0.8 μm can be found at the center of the rocking curve. This is about 200 times the escape depth for the evanescent wave emission effect described in Fig. 5.

With the angular and depth distribution of the fluorescence yield described by Eq. (7), the total yield observed by the detector (Eq. (2)) can be obtained through the integration of Eq. (7) over z and α, which gives the effective thickness $L(\theta)$ as

$$L(\theta) = \int_{\alpha_l}^{\alpha_u}\int_0^\infty y(\theta, \alpha, z)\, dz\, d\alpha$$

$$= \frac{1}{L_{OB}}\int_{\alpha_l}^{\alpha_u} \frac{I_{s,2}(\alpha)}{\mu_{z,1}(\theta) + \mu_{z,2}(\alpha)}\, d\alpha, \tag{9}$$

where the constant L_{OB} is an integration factor which normalizes $L(\theta)$ to unity at the off-Bragg (OB) condition where $R(\theta) = 0$ and $\mu_{z,1}(\theta) = \mu_{0,1}/\sin\theta_B$. The necessity of the integration over takeoff angle α in Eq. (9), which must be carried out numerically, depends on the instrumental resolution of angle α or the width $\Delta\alpha = \alpha_u - \alpha_l$, and the center position α_0 of $\Delta\alpha$. It can be avoided and replaced with its integrand calculated at α_0 if α_0 is far above the critical angle α_c or if $\Delta\alpha$ is small compared to α_c. This can be understood by plotting out the integrand $I_{s,2}(\alpha)/[\mu_{z,1}(\theta) + \mu_{z,2}(\alpha)] \approx I_{s,2}(\alpha)/\mu_{z,2}(\alpha)$ as a function of α. This is plotted as the $I_{out}(\alpha)$ curve in Fig. 5.

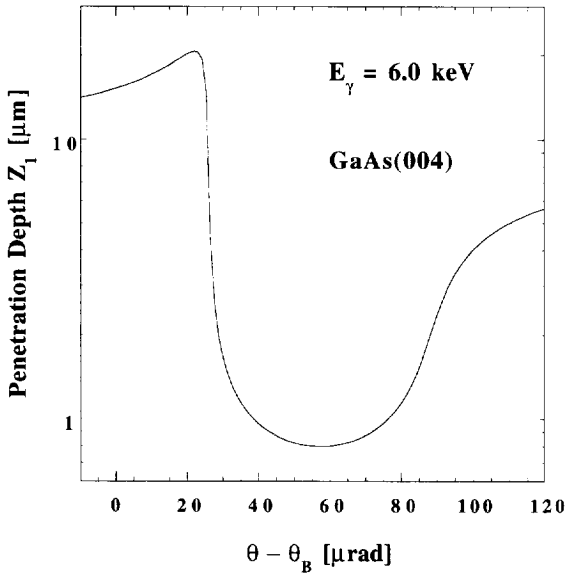

Fig. 6. The calculated angular dependence of the penetration depth of the primary X-ray for the GaAs(004) Bragg reflection at an X-ray energy of $E_\gamma = 6.00$ keV.

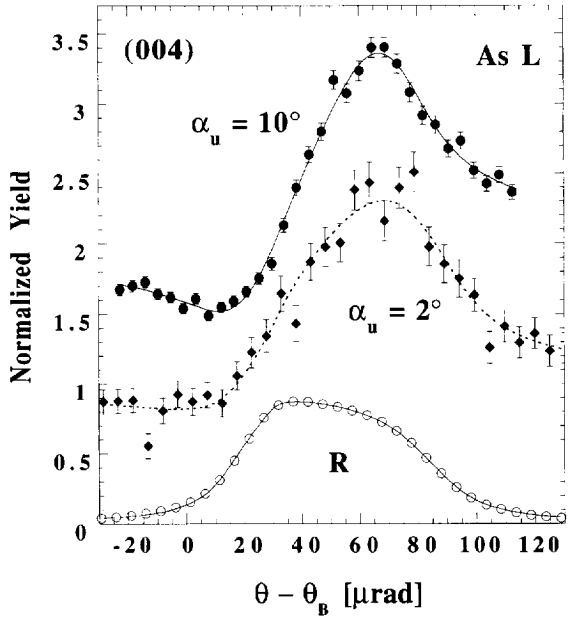

Fig. 7. The experimental XSW data and the best fits for the normalized As L fluorescence yields at $\alpha_u = 2°$ and 10° and the GaAs(004) reflectivity R versus angle θ. The 10° curve is offset by 1 for the purpose of clarity.

The low-takeoff angle XSW experiments were carried out at $\alpha_u = 4°$, 3° and 2°. Fig. 7 shows the As Lα fluorescence yields measured at $\alpha_u = 10°$ and 2°. The coherent fractions and coherent positions for arsenic and indium determined by χ^2 fit of Eq. (2) to the data measured at various takeoff angles are tabulated in Table 1. As evident in Fig. 7, as α_u approaches the critical angle $\alpha_c = 1.5°$, the fluorescence modulation amplitude gradually decreases and the yield maximum is shifted toward the low angle side of the rocking curve. This corresponds to a decrease in the coherent fraction and an increase in the coherent position. This change is due to the significant reduction of the As Lα escape depth near the critical angle which makes the As Lα signal more sensitive to the cap and less sensitive to the bulk GaAs. In the extreme case, where $\alpha_u = 2°$ and the maximum escape depth is about 120 Å, over 30% of the As yield is contributed by the cap. The coherent fraction f_c and coherent position P_c for arsenic in the cap can therefore be determined quantitatively by fitting the following modified yield equation to the fluorescence yield at $\alpha_u \sim \alpha_c$:

$$Y(\theta) = Y_{OB}\left\{1 + R(\theta) + 2\sqrt{R(\theta)}\left[f_s\cos(\nu(\theta) - 2\pi P_s)\frac{L_s}{L} + f_c\cos(\nu(\theta) - 2\pi P_c)\left(1 - \frac{L_s}{L}\right)\right]\right\} L. \quad (10)$$

The constant L is the effective thickness defined by Eq. (9) with $\alpha_i = 0$ and with $\mu_{z,1}(\theta)$ omitted (since $\mu_{z,1}(\theta) \ll \mu_{z,2}(\alpha)$ when α is near α_c). The constant L_s has the same definition as L except that the integration over depth starts at $z = t_c$ rather than $z = 0$. This accounts for the arsenic yield contributed by the substrate below the cap.

In Eq. (10), f_s and P_s are the substrate arsenic coherent fraction and coherent position. These values were determined to be $f_s = 0.81 \pm 0.01$ and $P_s = 1.00 \pm 0.01$ by the (004) XSW measurement at $\alpha_u = 10°$ (the solid line in Fig. 7), at which angle the escape depth is significantly larger than the cap thickness t_c and thus the cap contribution is negligible. The reasonably high coherent fraction (in comparison with the 0.89 GaAs(004) Debye–Waller factor) and the ideal bulk coherent position for arsenic at $\alpha_u = 10°$ indicate a highly ordered GaAs buffer layer where 90% of the arsenic atoms register with the bulk GaAs(004) planes.

The χ^2 fit of Eq. (10) to the $\alpha_u = 2°$ data with fixed parameters α_u, t_c, f_s and P_s (the dashed line in Fig. 7) gives $f_c = 0.64 \pm 0.12$ and $P_c = 0.33 \pm 0.03$, corresponding to a 0.47 ± 0.04 Å displacement of the cap layer (h_{cap}) in the growth direction with respect to the bulk (004) planes. This result is in good agreement with our measured indium (004) position, which predicts $h_{cap} = 2h_{In} = 0.44$ Å, as depicted by the ball and stick model in Fig. 2. This consistency between our measurements of the cap

Table 1
Result of the (004) XSW measurements and calculated escape depths Z_2 at $\alpha_u = 2°, 3°, 4°$ and 10°. The coherent fractions f and coherent positions P are determined by χ^2 fit of Eq. (2) to the data with $L(\theta)$ defined by Eq. (9) for As and with $L(\theta) = 1$ for In

α_u		10°	4°	3°	2°
	Z_2 (Å)	900	330	230	120
As	f	0.81 ± 0.01	0.70 ± 0.01	0.65 ± 0.01	0.48 ± 0.03
	P	1.00 ± 0.01	1.01 ± 0.01	1.024 ± 0.01	1.062 ± 0.01
In	f	0.43 ± 0.03	0.44 ± 0.02	0.42 ± 0.02	0.43 ± 0.02
	P	1.154 ± 0.01	1.151 ± 0.01	1.159 ± 0.01	1.156 ± 0.01

displacement and the In position has an important implication with respect to characterizing the overall strain of a buried film which is thicker than 1 ML. In such a case, the multiple positions of the impurity atoms in the strained layer will reduce the coherent fraction and thus obscure the structural information gained from the coherent position of the impurity. However, by measuring the position of the cap layer with XSW, one can obtain the cumulative lattice displacement within the strained layer.

In future studies of this type, we will use a thicker (100–200 Å) cap layer. In this case, it will be possible to eliminate essentially the substrate signal at $\alpha_u \sim \alpha_c$ and directly measure the positions of the atoms in the cap. Since $\mu_{z,1}(\theta) \ll \mu_{z,2}(\theta)$ in Eq. (9) and only one coherent position needs to be considered in Eq. (10), Eq. (2) with $L(\theta) = 1$ becomes a proper formula for describing the fluorescence yield in this case, which implies that atoms distributed within the depth of a few hundred angstroms can be treated as if they were on the surface. Consequently, the uncertainties about the cap layer thickness t_c and the upper limit of the emission takeoff angle α_u can be entirely removed from the data interpretation. With these advantages realized, the XSW method can be applied as a highly precise nondestructive probe for studying buried heteroepitaxial structures as well as interfacial segregation.

In summary, a GaAs/1 ML InAs/GaAs(001) heterostructure grown by MBE was characterized by X-ray standing waves. The measured strain in the InAs layer agrees with the macroscopic elasticity theory in the 1 ML limit. By controlling the emission takeoff angle of the As Lα fluorescence, the evanescent-wave-emission effect was used in combination with the XSW effect to study the epitaxy of the heterostructure as a function of depth. We used this depth-selective XSW method to measure the displacement of the GaAs cap layer in the growth direction, and directly related this displacement to the perpendicular strain in the InAs layer.

Acknowledgements

This work was supported by the US Department of Energy under contract No. W-31-109-ENG-38 to Argonne National Laboratory, contract No. DE-AC02-76CH00016 to the National Synchrotron Light Source at Brookhaven National Laboratory, and by the National Science Foundation under contract No. DMR-9120521 to the MRC at Northwestern University. PFL is partially supported by the National Institutes of Health under award No. IR01KD45295-01. Additional support was provided by the National Institute of Standards and Technology.

References

[1] A. Zunger and D.M. Wood, J. Crystal Growth 98 (1989) 1. See also D.M. Wood and A. Zunger, Phys. Rev. B. 40 (1989) 4062.
[2] O. Madelung (ed.), Semiconductors: Group IV Elements and III–V Compounds (Springer, Berlin, 1991).
[3] O. Brandt, K. Ploog, R. Bierwolf and M. Hohenstein, Phys. Rev. Lett. 68 (1992) 1339.
[4] C. Giannini, L. Tapfer, S. Lagomarsino, J.C. Boulliard, A. Taccoen, B. Capelle, M. Ilg, O. Brandt and K.H. Ploog, Phys. Rev. B 48 (1993) 11496.
[5] J.E. Bernard and A. Zunger, Appl. Phys. Lett. 65 (1994) 165.
[6] J.C. Woicik, J.G. Pelligrino, S.H. Southworth, P.S. Shaw, B.A. Karlin, C.E. Bouldin and K.E. Miyano, Phys. Rev. B 52 (1995) R2281.
[7] This energy scan is equivalent to scanning the angle of the sample substrate about the Bragg angle, and the abscissas

of the XSW data will be expressed as angular deflections for convenience.
[8] For a review of dynamical diffraction theory, see B.W. Batterman and H. Cole, Rev. Mod. Phys. 36 (1964) 681.
[9] L. Tapfer and K. Ploog, Phys. Rev. B 40 (1989) 9802.
[10] T. Takahashi and S. Kikuta, J. Phys. Soc. Japan 47 (1979) 620.
[11] M.J. Bedzyk, G. Materlik and M.V. Kovalchuk, Phys. Rev. B 30 (1984) 4881.
[12] R.S. Becker, J.A. Golovchenko and J.R. Patel, Phys. Rev. Lett. 50 (1983) 153.
[13] For example, M. Born and E. Wolf, Principles of Optics (Pergamon Press, New York, 6th ed., 1993).
[14] B.W. Batterman, Phys. Rev. 133 (1964) A759.